Beam steering and topological transformations driven by interactions between a discrete vortex soliton and a discrete fundamental soliton

Xuetao Gan, Peng Zhang,* Sheng Liu, Fajun Xiao, and Jianlin Zhao†

Key Laboratory of Space Applied Physics and Chemistry, Ministry of Education, and Shaanxi Key Laboratory of Optical Information Technology, School of Science, Northwestern Polytechnical University, Xi'an 710072, China

(Received 12 August 2013; published 29 January 2014)

We study coherent and incoherent interactions between a discrete vortex soliton and a discrete fundamental soliton in two-dimensional photonic lattices, which present a scheme for all-optical routings and topological transformations of vorticities. Due to the multilobe intensity and $\pi/2$-phase delay between each two lobes of the discrete vortex soliton, the coherent soliton interactions allow both solitons to evolve into localized states with a single lobe on multiple different possible destination ports, which depend on the initial phase of the discrete fundamental soliton. We show that charge flippings of phase singularities and orbital angular momentum transfer can occur during the coherent interactions between the two solitons. For incoherent interactions, by controlling the relative powers of the two solitons, we reveal that soliton steering can be realized by either attracting the discrete fundamental soliton to four ports or localizing the four-lobe discrete vortex soliton into a ring soliton.

DOI: 10.1103/PhysRevA.89.013844 PACS number(s): 42.65.Tg, 05.45.Yv, 42.82.Et, 03.75.Lm

I. INTRODUCTION

Light propagation in linear and nonlinear optical waveguide arrays has been attracting great research interest [1,2] over the last decade; this represents a host for exploring discrete physics phenomena in optics, including anomalous diffraction and refraction [3–5], Anderson localization [6], Rabi oscillation [7], and Zener tunneling [8], as well as photonic topological insulators [9]. With a balance of nonlinear trapping and discrete diffraction, an optical beam launched into a single site of a waveguide array can form a discrete fundamental soliton (DFS) [10–13]. The interactions between DFSs have been demonstrated to perform the blocking, deflecting, and routing of optical beams along defined paths in the waveguide-array networks [14–17]. Optical vortices associated with phase dislocations and topological characters exhibit many interesting features, such as helical phase structure, doughnut intensity profile, and orbital angular momentum (OAM), which promise interesting nonlinear evolution dynamics [18,19] and a wide range of applications [20–22]. In bulk nonlinear materials, vortex solitons with a dark hole embedded in a uniform background were observed under saturable self-defocusing nonlinearity [19,23,24]. In a self-focusing nonlinear medium, although vortex beams tend to break up into bright filaments due to the azimuthal modulation instabilities, vortex-ring solitons can be formed with the presence of a nonlocal nonlinearity [25,26]. In two-dimensional (2D) nonlinear lattices induced optically and magnetically, vortices can localize into four [27,28] or more [29–31] sites and form discrete vortex solitons (DVSs). Soliton interactions involving DVSs promise more possible soliton algebra for light controlling due to the complex intensity distributions and topological characters [32]. In this paper, we study the coherent and incoherent interaction dynamics between a DVS and a DFS in an optically induced photonic lattice. The multilobe intensity and $\pi/2$-phase delay between each two lobes of DVSs enable the controllable energy and angular momentum transfer during the interactions with DFSs. In comparison with the interactions of two DFSs, the interactions between a DVS and a DFS enable the evolutions of both solitons into single lobes on multiple possible destination sites, providing a promising approach for all-optical routings.

II. GOVERNING EQUATIONS AND SOLITON SOLUTIONS

The 2D photonic lattice is optically induced in a photorefractive crystal with a saturable screening nonlinearity [11]. The paraxial propagation dynamics of a slowly varying optical envelope $B(x, y, z)$ along the z axis in the photonic lattice is governed by the nondimensional nonlinear Schrödinger equation [33],

$$i\frac{\partial B}{\partial z}+\frac{1}{2}\left(\frac{\partial^2 B}{\partial x^2}+\frac{\partial^2 B}{\partial y^2}\right)-\frac{E_0}{1+I_l+I_p}B=0, \quad (1)$$

where E_0 is the applied dc electrical field, and I_p and I_l are the intensities of the extraordinarily polarized probe beam and the ordinarily polarized lattice-writing beam normalized by the dark irradiance, respectively. Figure 1(a) shows the square photonic lattice determined by $I_l = I_{l0}\cos^2(\pi x/d)\cos^2(\pi y/d)$, which can be induced by four interfering plane waves experimentally [12]. Here, I_{l0} and d are the peak intensity and period of the lattice, which are chosen as $I_{l0} = 1$ and $d = 4$ in our numerical simulations. In view of typical experimental conditions [17], here $E_0 = 1$, $x(y) = 1$, and $z = 1$ correspond to 1000 V/cm, 6.4 μm, and 0.88 mm, respectively.

The solitary solutions of Eq. (1) are sought in the form of $B(x, y, z) = b(x, y)\exp(i\beta z)$, where β is the propagation constant, and $b(x, y)$ satisfies

$$\frac{1}{2}\left(\frac{\partial^2 b}{\partial x^2}+\frac{\partial^2 b}{\partial y^2}\right)-\frac{E_0}{1+I_l+I_p}b=\beta b. \quad (2)$$

A Fourier iteration method [34] is applied to solve Eq. (2). Using a trial solution as $b(r,\theta) = r^m\exp(-r^2/36 + im\theta)$, where (r, θ) are the polar coordinates and m is the topological

*Present address: NSF Nanoscale Science and Engineering Center, University of California, Berkeley, CA 94720, USA.

†Corresponding author: jlzhao@nwpu.edu.cn

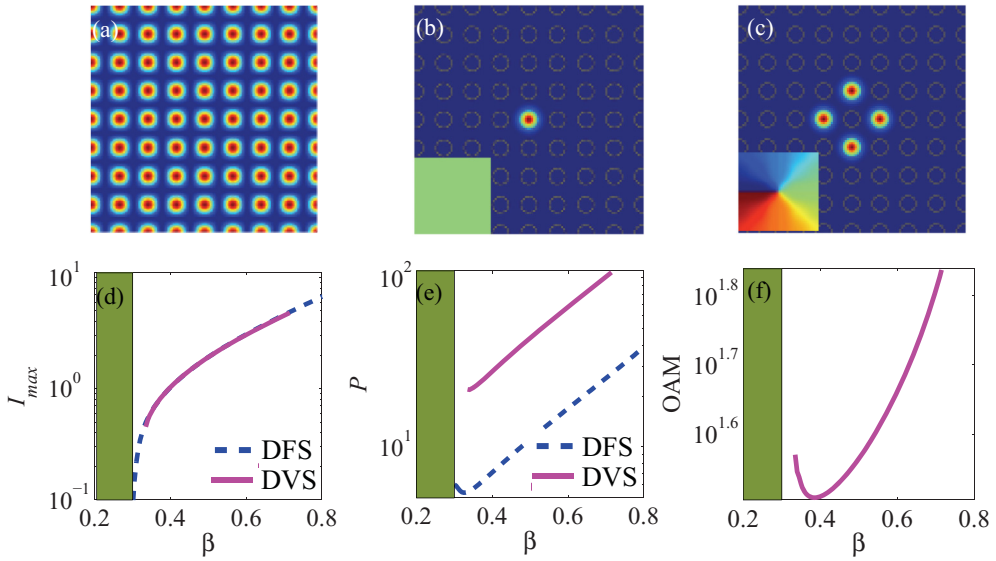

FIG. 1. (Color online) (a) Cross section of 2D square lattice; (b), (c) intensity and phase (inset) distributions of DFS and single-charged DVS at $\beta = 0.55$; (d)–(f) peak intensity, power, and OAM of solitons versus β, where dashed and solid lines correspond to the DFS and DVS, respectively. Filled area: the first Bloch band.

charge, we can obtain the on-site DFS and single-charged DVS with $m = 0$ and 1, respectively.

Figures 1(b)–1(f) display the solitons calculated under an applied electrical field of $E_0 = 1.5$, which provides a focusing nonlinearity on the probe beam. Both DFSs and DVSs reside in the semi-infinity band gap. Different from DFSs, DVSs disappear when β ($\beta \leq 0.35$) closes to the band edge of the first Bloch band, which indicates that DVSs are not bifurcated from the Bloch waves at the band edge [34]. In addition, the DVSs only exist in a propagation constant range of $0.35 < \beta < 0.69$ due to the instabilities [34]. Figures 1(b) and 1(c) depict the intensity and phase (insets) structures of a DFS and an on-site DVS at $\beta = 0.55$. Unlike DFS, the DVS has four lobes showing relative phase changes between each other in steps of $\pi/2$. Moreover, the 2π-winding phase around the central singularity indicates the single-charged phase dislocation of the DVS. We plot the peak intensities $I_{\max}$ and powers P of the two solitons versus β in Figs. 1(d) and 1(e). Here, the power is defined as $P = \int\int |b|^2 dxdy$. It can be seen that the peak intensities of DFSs and DVSs are the same monotonically increasing function of β. The power diagrams show inflexions for both solitons, implying the critical β values for changing the soliton stability [34]. Resulting from the vorticity and singularity, the DVSs possess OAMs and their dependences on β are shown in Fig. 1(f), where the OAM is calculated by $M = i\int\int(b^*\nabla_\perp b - b\nabla_\perp b^*)dxdy$ [35], and b^* denotes the conjugation of b.

The interactions of the above solitons are addressed by configuring a DFS in the central site of an on-site DVS. To study the interaction dynamics, we simulate the mutual propagations of DFS (B_1) and DVS (B_2) in the photonic lattice according to the following coupled-mode equations [17]:

$$i\frac{\partial B_{1,2}}{\partial z} + \frac{1}{2}\left(\frac{\partial^2 B_{1,2}}{\partial x^2} + \frac{\partial^2 B_{1,2}}{\partial y^2}\right) - \frac{E_0}{1 + I_l + I_p}B_{1,2} = 0. \tag{3}$$

For the coherent and incoherent interactions, the total intensities of the probe beams I_p are governed by the two solitons in the form of $I_p = |B_1 + B_2\exp(i\varphi)|^2$ and $|B_1|^2 + |B_2|^2$, respectively, where φ is the initial phase of DFS.

III. COHERENT INTERACTIONS

The coherent soliton interaction is sensitive to the phase difference between the solitons [15,36,37]. To ensure a reliable interaction process, we employ the DVS and DFS having the same propagation constant to maintain their relative phase difference during the propagation. Since the phase structure of the DVS has multiple values on the four lobes, it is difficult to define the phase difference between the DVS and DFS. Here, we study their coherent interactions by changing the initial phase of the DFS as $\varphi = 0$, $\pi/2$, π, and $3\pi/2$, respectively, which correspond to the $\pi/2$-step phase structure of the DVS. Figure 2 shows the interaction result of two solitons at $\beta = 0.55$ in the case of $\varphi = 0$. Figures 2(a)–2(c) depict the input soliton beams, the three-dimensional (3D) interaction trajectories in a propagation length of $z = 100$, and the output beams of the DFS (1) and the DVS (2), respectively. The result reveals that both solitons evolve into localized states via the coherent interaction: the DFS shifts and localizes to the port below the center lattice site; the DVS decays from the four-site profile to a single bright lobe on the bottom port. Moreover, the two evolved solitons present incessant rotations during their propagations on the localized site. From the phase structures shown in the insets of Figs. 2(a) and 2(c), one can tell that the output DFS presents a helical phase singularity, whereas no singularity appears in the output DVS field. The rotational propagations and evolutions of phase singularities of the solitons indicate the topological transformations of vorticities during the coherent interaction.

To analyze the above interaction dynamics, we depict the intensity profiles of DFS (upper row) and DVS (lower row) at different propagation lengths of $z = 10$, 20, and 30 in Figs. 3(a)–3(c), where the insets show the phase structures. In Fig. 2(a), the phase structures of the input beams reveal that

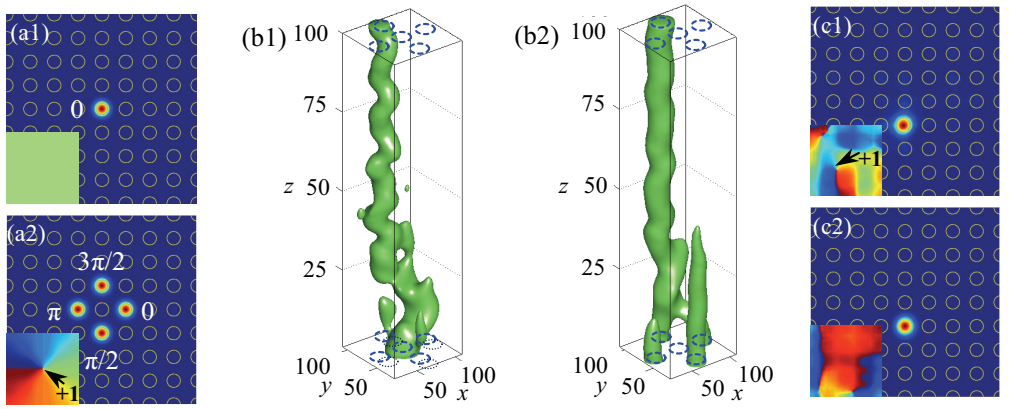

FIG. 2. (Color online) Coherent interaction of DVS and DFS at $\beta = 0.55$ in the case of $\varphi = 0$. (a) Input solitons; (b) iso-surface plot showing soliton interaction trajectories within the propagation length of $z = 100$; (c) output beams of (1) DFS and (2) DVS, where the insets show the phase structures of the solitons.

the DFS has an identical phase with the right lobe of the DVS. As indicated in the coupled-mode equation of Eq. (3), the intensity I_p in the coupling region of the two in-phase soliton lobes is increased due to the constructive interference, which leads to an increase in the refractive index in that region. This in turn constructs an attractive force between the two soliton lobes [15,36,37]. On the other hand, the DFS is out of phase with the left lobe of the DVS and would move further to the right due to the repulsion force [15,36,37]. As a result, the DFS is transferred into the adjacent site to the right, as shown in Fig. 3(a1). On the other hand, the attraction of the DFS breaks up the balance of energy flow of the DVS among the four lobes [38], resulting in the lobes rotate around the center lattice-site for the inherent OAM [Fig. 3(a2)]. As the original right lobe of the DVS rotates into the bottom site, the DFS is dragged into the bottom site gradually by the sustained attraction, as shown in Figs. 3(b) and 3(c). In the further propagation, the solitons' rotations are blocked by the lattice potential of the bottom site, presenting localized states for both solitons, as shown in Figs. 2(b) and 2(c).

An OAM transfer is expected in the coherent interaction due to the breakup of DVS and rotational propagations of the final localized solitons. We plot the calculated OAMs of DFS, DVS, and sum of them versus the propagation distance in Fig. 3(d), which are denoted as the dotted, dashed, and solid lines, respectively. It is revealed that, transferring OAM from the DVS, the DFS has a gradually increased OAM, which reaches a maximum at about $z = 20$. Correspondingly, the OAM of the DVS decreases to a minimum. Next, a reverse OAM transfer process arises; i.e., the DFS transfers its OAM back to the DVS until its value becomes zero around the propagation length of $z = 30$, resulting in a maximum OAM of the DVS. The further propagation preserves the oppositely altering trends of OAMs of the two solitons, implying the continuously mutual angular momentum transfer. However, the sum of OAMs of the two solitons is not conservative due to the interplay with the nonlinearity and periodicity of lattice potential [39,40].

In optical vortices, helical phase singularities with topological charge are responsible for the OAM. Following the OAM transfer, we observe charge flippings of the phase singularities in the two solitons. Similar to the analysis of topological transformation of vortex beams in Ref. [40], we define the topological charge of the input DVS equal to $+1$, showing a clockwise helical phase dislocation. At the propagation distance of $z = 20$, the field of DFS appears as a clockwise helical phase dislocation at the center, signifying a singularity with $+1$ charge, as shown in Fig. 3(b1). Meanwhile, the charge of DVS becomes zero as its singularity fades away [Fig. 3(b2)]. At $z = 30$, while two phase dislocations

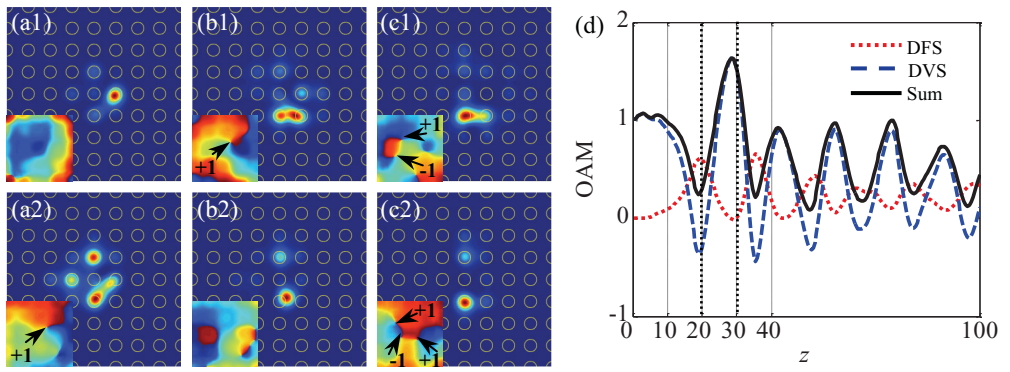

FIG. 3. (Color online) (a)–(c) Intensity and phase (insets) distributions of the DFS (upper row) and DVS (lower row) during the coherent interaction at $z = 10$, 20, and 30; (d) OAMs of DFS, DVS, and their sum, which are marked as dotted, dashed, and solid lines, respectively.

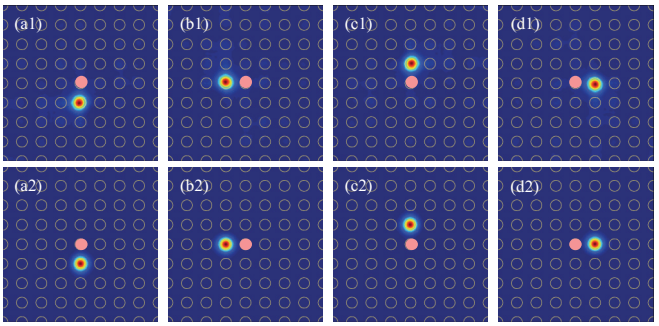

FIG. 4. (Color online) Output intensity profiles of the coherent interactions between DFS (upper row) and DVS (lower row) at $z = 100$, where (a)–(d) correspond to the cases of $\varphi = 0, \pi/2, \pi$, and $3\pi/2$, respectively.

are present in the DFS shown in Fig. 3(c1), their opposite rotation directions flip the total topological charge into zero. Correspondingly, the DVS has a charge of $+1$ after the algebraic sum of three phase dislocations with $+1$, -1, and $+1$ [Fig. 3(c2)]. Combining with Fig. 3(d), the results indicate a good agreement between the charge flipping and OAM transfer. This topological transformation is also found at other propagation distances.

We further study the interactions between the DVS and DFS with initial phases of $\varphi = \pi/2$, π, and $3\pi/2$, respectively. Due to the symmetry of the four lobes of the DVS, similar evolution processes are observed with the same dynamics of $\varphi = 0$. Output intensity profiles of the DFS (upper row) and DVS (lower row) at $z = 100$ are displayed in Fig. 4, where (a)–(d) correspond to the cases of $\varphi = 0, \pi/2, \pi$, and $3\pi/2$, respectively. With the symmetry of the system, both solitons ultimately evolve into single lobes on the lower, left, upper, and right ports relative to the center lattice site (the pink point in figures), respectively. The results demonstrate the multiple possible destination ports of the soliton steering provided by the four lobes of DVS, and the desired route can be engineered by controlling the initial phase of DFS. This could be interesting for the phase-dependent optical routing and switching. The interactions between the DVS and DFS at other propagation constants in the range of $0.35 < \beta < 0.69$ are also simulated, which show the same output ports as that at $\beta = 0.55$. The results indicate, over the DVS existing range, both DVSs and DFSs have moderate powers that enable their coherent interactions to depend on the initial phase of the DFS strongly [37].

The robustness of the interaction dynamics is then tested by adding white noise into the input DVS and DFS [28]. The simulation results reveal the coherent interaction can hold its dynamics when the power of the white noise is less than 15% of the power of the input solitons. Note that the results discussed above involve solitons with the same propagation constant. If the propagation constants of the solitons are different, their interactions would present incoherent interaction dynamics because the relative phase varies much faster than the response speed of the photorefractive effect [36].

IV. INCOHERENT INTERACTIONS

The incoherent soliton interactions are independent of the phase difference and always yield attractive forces due to the increased refractive index in the soliton overlapping region [36], as indicated in Eq. (3), which enable effective optical blockings and routings [41]. With the benefit of the four lobes and OAM of DVSs, more distinctive results are expected in the incoherent interactions between DVSs and DFSs. We study the incoherent interactions by fixing the DVS and changing the DFSs with different input powers. Figure 5 shows the interaction results between DFS (1) and DVS (2), where Fig. 5(a) depicts the intensity profiles of the input solitons. Here, the DVS is chosen at $\beta = 0.55$ with an input power of 51.6. Figures 5(b) and 5(c) display the 3D interaction trajectories and the output profiles of the solitons at $z = 100$ for the DFS having a lower power of 12.6 ($\beta = 0.55$). The results reveal the DFS is dragged into four lobes with the same power of 3.2, indicating a possible four-port soliton-routing, where the DVS maintains its four-lobe profile. However, when the DFS power exceeds a threshold value (14.9 in our parameters), the attraction force from the DVS is not strong enough to break the localization of the DFS. Choosing a DFS with power of 26.2, we obtain the interaction results shown in Figs. 5(d) and 5(e). Accompanying with a small broadening of the DFS, the DVS is constricted and localized onto the center lattice-site. The evolved DVS showing a stable ring profile is different from a ring-DVS with high intensity demonstrated in Ref. [29] and can be understood as composite solitons with the DFS [36,42]. The OAM transfer between the two solitons is not observed

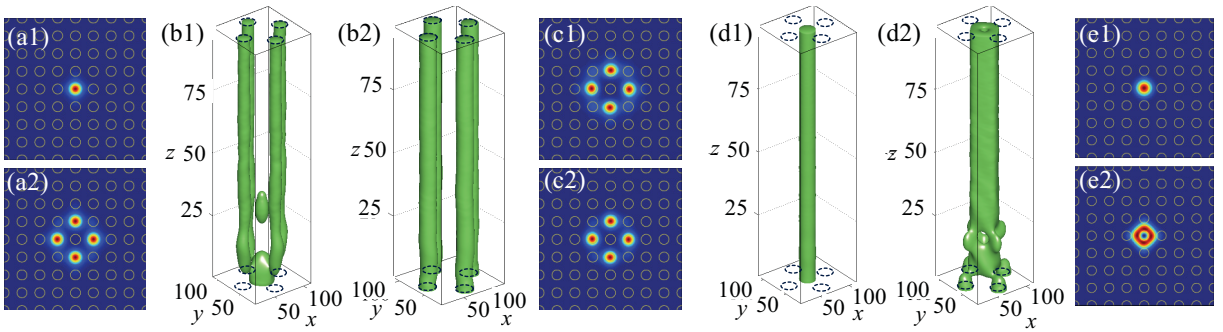

FIG. 5. (Color online) Incoherent interactions between a DVS (2) with power of 51.6 and DFSs (1) with different powers. (a) Input solitons; (b) iso-surface plot showing 3D soliton interaction trajectories; (c) output of the solitons at the propagation length of $z = 100$, where the input power of DFS is 12.6; (d) and (e) are similar to (b) and (c) except the input power of DFS is 26.2.

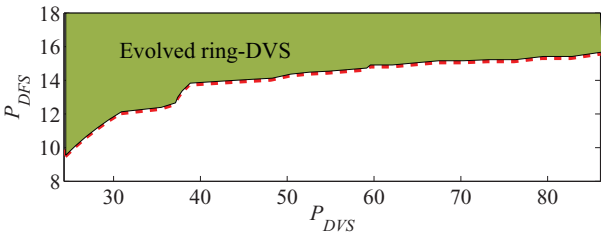

FIG. 6. (Color online) Power thresholds of the DFS for the evolutions of DVSs into ring solitons versus the DVS powers (P_{DVS}) in the incoherent interactions, denoted by the dashed line. Filled area: DFS powers (P_{DFS}) enabling the DVSs to evolve into ring solitons.

due to the phase-independence, however, the OAM of DVS arises a transfer from four lobes into a single port.

We further simulate the incoherent interactions using other existed DVSs with different powers. The results show similar soliton evolution behaviors as that shown in Fig. 5, which depend on the input powers of the DFSs. For DVSs with different powers, we calculate the power thresholds of the DFSs enabling the DVSs evolve into ring solitons, as plotted in Fig. 6. The monotonously increased curve with respective to DVS powers (P_{DVS}) indicates high DFS powers (P_{DFS}) are required to break the localization of a high-power DVS and re-confine it into a ring on the center lattice-site. Compared with the coherent interaction, the independence of relative phase makes the incoherent interaction more conveniently to arrange. However, the incoherent interactions are not stable when the input solitons are perturbed by noises.

V. CONCLUSION

In conclusion, we have demonstrated soliton-steering and topological transformation behaviors during the coherent and incoherent interactions between DVS and DFS in 2D photonic lattices. It has been shown that the nontrivial phase and intensity structures of the DVS offer an efficient beam routing strategy with discretized destination ports. By controlling the initial DFS phase, the coherent interaction allows solitons to evolve into different desired sites. The observed charge-flipping and OAM transfer dynamics during the soliton interactions could be interesting for the OAM-based information processing in nonlinear waveguide arrays [43]. In addition, we have revealed that incoherent interactions may result in composite solitons being either a four-lobe DFS or a ring DVS. These rich interactions open up prospects for all-optical routings by designing the interactions between different higher-order solitons [44], and soliton controllings in other nonlinear periodic structures such as photonic crystals [45] and Bose-Einstein condensates [46].

ACKNOWLEDGMENTS

This work was supported by the 973 Program (Grant No. 2012CB921900), the National Natural Science Foundations of China (Grants No. 61205001 and No. 61377035), the Natural Science Basic Research Plan in Shaanxi Province of China (Grant No. 2012JQ1017).

[1] Y. V. Kartashov, V. A. Vysloukh, and L. Torner, Prog. Opt. **52**, 63 (2009).
[2] Z. Chen, M. Segev, and D. N. Christodoulides, Rep. Prog. Phys. **75**, 086401 (2012).
[3] T. Pertsch, T. Zentgraf, U. Peschel, A. Bräuer, and F. Lederer, Phys. Rev. Lett. **88**, 093901 (2002).
[4] C. R. Rosberg, D. N. Neshev, A. A. Sukhorukov, Y. S. Kivshar, and W. Krolikowski, Opt. Lett. **30**, 2293 (2005).
[5] P. Zhang, C. Lou, S. Liu, J. Zhao, J. Xu, and Z. Chen, Opt. Lett. **35**, 892 (2010).
[6] M. Segev, Y. Silberberg, and D. N. Christodoulides, Nat. Photon. **7**, 197 (2013).
[7] K. Shandarova, C. E. Rüter, D. Kip, K. G. Makris, D. N. Christodoulides, O. Peleg, and M. Segev, Phys. Rev. Lett. **102**, 123905 (2009).
[8] H. Trompeter, T. Pertsch, F. Lederer, D. Michaelis, U. Streppel, A. Bräuer, and U. Peschel, Phys. Rev. Lett. **96**, 023901 (2006).
[9] M. C. Rechstman, J. M. Zeuner, Y. Plotnik, Y. Lumer, D. Podolsky, F. Dreisow, S. Nolte, M. Segev, and A. Szameit, Nature **496**, 196 (2013).
[10] D. N. Christodoulides and R. I. Joseph, Opt. Lett. **13**, 794 (1988).
[11] N. K. Efremidis, S. Sears, D. N. Christodoulides, J. W. Fleischer, and M. Segev, Phys. Rev. E **66**, 046602 (2002).
[12] J. W. Fleischer, M. Segev, N. K. Efremidis, and D. N. Christodoulides, Nature **422**, 147 (2003).
[13] Z. Chen, H. Martin, E. D. Eugenieva, J. Xu, and A. Bezryadina, Phys. Rev. Lett. **92**, 143902 (2004).
[14] R. Keil, M. Heinrich, F. Dreisow, T. Pertsch, A. Tünnermann, S. Nolte, D. N. Christodoulides, and A. Szameit, Sci. Rep. **1**, 94 (2011).
[15] J. Meier, G. I. Stegeman, Y. Silberberg, R. Morandotti, and J. S. Aitchison, Phys. Rev. Lett. **93**, 093903 (2004).
[16] E. Smirnov, C. E. Ruter, M. Stepic, V. Shandarov, and D. Kip, Opt. Express **14**, 11248 (2006).
[17] S. Liu, Y. Hu, P. Zhang, X. Gan, F. Xiao, C. Lou, D. Song, J. Zhao, J. Xu, and Z. Chen, Opt. Lett. **36**, 1167 (2011).
[18] X. Gan, P. Zhang, S. Liu, Y. Zheng, J. Zhao, and Z. Chen, Opt. Express **17**, 23130 (2009).
[19] X. Gan, P. Zhang, S. Liu, F. Xiao, and J. Zhao, Chin. Phys. Lett. **25**, 3280 (2008).
[20] G. Molina-Terriza, J. P. Torres, and L. Torner, Nat. Phys. **3**, 305 (2007).
[21] M. Padgett and R. Bowman, Nat. Photon. **5**, 343 (2011).
[22] G. Foo, D. M. Palacios, and G. A. Swartzlander, Jr., Opt. Lett. **30**, 3308 (2005).
[23] Z. Chen, M. Segev, D. W. Wilson, R. E. Muller, and P. D. Maker, Phys. Rev. Lett. **78**, 2948 (1997).
[24] Z. Chen, M. F. Shih, M. Segev, D. W. Wilson, R. E. Muller, and P. D. Maker, Opt. Lett. **22**, 1751 (1997).
[25] C. Rotschild, O. Cohen, O. Manela, M. Segev, and T. Carmon, Phys. Rev. Lett. **95**, 213904 (2005).

[26] D. Briedis, D. Petersen, D. Edmundson, W. Krolikowski, and O. Bang, Opt. Express **13**, 435 (2005).
[27] D. N. Neshev, T. J. Alexander, E. A. Ostrovskaya, Y. S. Kivshar, H. Martin, I. Makasyuk, and Z. Chen, Phys. Rev. Lett. **92**, 123903 (2004).
[28] J. W. Fleischer, G. Bartal, O. Cohen, O. Manela, M. Segev, J. Hudock, and D. N. Christodoulides, Phys. Rev. Lett. **92**, 123904 (2004).
[29] J. D. Wang and J. K. Yang, Phys. Rev. A **77**, 033834 (2008).
[30] H. Leblond, B. A. Malomed, and D. Mihalache, Phys. Rev. A **83**, 063825 (2011).
[31] C. Mejia-Cortes, J. M. Soto-Crespo, M. I. Molina, and R. A. Vicencio, Phys. Rev. A **82**, 063818 (2010).
[32] Z. Xu, Y. V. Kartashov, L. C. Crasovan, D. Mihalache, and L. Torner, Phys. Rev. E **71**, 016616 (2005).
[33] A. A. Zozulya and D. Z. Anderson, Phys. Rev. A **51**, 1520 (1995).
[34] J. Yang and Z. H. Musslimani, Opt. Lett. **28**, 2094 (2003).
[35] M. S. Soskin, V. N. Gorshkov, M. V. Vasnetsov, J. T. Malos, and N. R. Heckenberg, Phys. Rev. A **56**, 4064 (1997).
[36] G. I. Stegman and M. Segev, Science **286**, 1518 (1999).
[37] F. J. Xiao, P. Zhang, S. Liu, and J. L. Zhao, J. Opt. A **13**, 105101 (2011).
[38] T. J. Alexander, A. A. Sukhorukov, and Y. S. Kivshar, Phys. Rev. Lett. **93**, 063901 (2004).
[39] M. S. Petrović, D. M. Jović, M. R. Belić, and S. Prvanović, Phys. Rev. A **76**, 023820 (2007).
[40] A. Bezryadina, D. N. Neshev, A. S. Desyatnikov, J. Young, Z. Chen, and Y. S. Kivshar, Opt. Express **14**, 8317 (2006).
[41] J. Meier, G. I. Stegeman, D. N. Christodoulides, R. Morandotti, H. Yang, G. Salamo, M. Sorel, Y. Silberberg, and J. S. Aitchiso, Opt. Lett. **30**, 3174 (2005).
[42] E. A. Ostrovskaya, Y. S. Kivshar, D. V. Skryabin, and W. J. Firth, Phys. Rev. Lett. **83**, 296 (1999).
[43] J. Wang, J. Yang, I. M. Fazal, N. Ahmed, Y. Yan, H. Huang, Y. Ren, Y. Yue, S. Dolinar, M. Tur, and A. E. Willner, Nat. Photon. **6**, 488 (2012).
[44] Y. Kartashov, B. Malomed, and L. Torner, Rev. Mod. Phys. **83**, 247 (2011).
[45] A. Ferrando, M. Zacarés, and M. A. García-March, Phys. Rev. Lett. **95**, 043901 (2005).
[46] E. A. Ostrovskaya and Y. S. Kivshar, Phys. Rev. Lett. **93**, 160405 (2004).